ADVANCED OPTICAL MATERIALS
www.advopticalmat.de

Transparent Light-Emitting Electrochemical Cells

*Lorenzo Mardegan, Abhyuday Paliwal, Kassio P. S. Zanoni, Daniel Tordera, and Henk J. Bolink**

Single layer light-emitting electrochemical cells (LECs) are amongst the simplest electroluminescent devices and operate with air-stable electrodes. Transparent light-emitting devices are of great interest as they can enable new applications in consumer electronics. In this work, a transparent ionic transition metal complex based LEC is fabricated by developing a transparent top contact based on tin (IV) oxide (SnO_2) and indium-tin oxide, processed by low-temperature atomic layer deposition and pulsed laser deposition, respectively. The resulting devices present transparency in excess of 75% over the full visible spectrum (380–750 nm), with 82% transmission at the emission peak (563 nm). The devices emit from the front and the rear with high luminance (260 cd m^{-2}) and long lifetime (176 h). These parameters place them among the highest performing single layer transparent electroluminescent devices.

1. Introduction

In recent years, new display technologies have emerged, and with them, the need for development of properties such as large area, stretchability, or transparency in organic light-emitting devices (OLEDs).[1,2] In particular, for semitransparent OLEDs, the requirements for the cathode are a high light transmittance (over 80%) and a low sheet resistance (R_s).[3] The realm of transparent electrodes is vast and in continuous progress, nonetheless the most common materials and structures are transparent conductive oxides (TCOs), very thin films of metals or alloys (e.g., Ag, Au, Ag:Al, Mg:Ag), multilayer metal thin film based cathodes (e.g., dielectric/metal/dielectric, metal/metal), nano arrays (e.g., carbon based electrodes and metal nanowire electrodes) and conductive polymers (e.g., poly(3,4-ethylenedioxythiophene): polystyrenesulfonate (PEDOT:PSS)).[4–6] TCOs are the preferred materials as transparent bottom electrodes, as they possess a high conductivity and there are barely any process limitations since they are often deposited on glass or plastic substrates that endure the harsh conditions during the TCO deposition via, for example, magnetron sputtering. The use of TCOs as transparent top electrodes on thin organic semiconductor based devices requires, however, more attention, particularly regarding the chemical and processing compatibility with the underlying thin (usually <500 nm) organic semiconductor layers. Additionally, the alignment of the TCO conduction band with the energy of the molecular orbitals of the organic semiconductor is important. These requirements have limited the widespread usage of TCO as top electrode in organic semiconductor devices.[5] For example, the sputtering of TCO directly on top of device stacks can damage underlying charge transport layers or the active materials themselves, reducing their performances and lifetimes.[7] The use of indium-tin oxide (ITO) as top electrode in semitransparent devices has been studied in LEDs and OLEDs. Recent publications show that to avoid sputtering damage on the organic layers a buffer layer has to be included, usually ZnO nanoparticles or ultra-thin metal films, as well as carefully choosing the deposition conditions, taking into account the trade-off between the sheet resistance and the damage.[8–13] One of the most efficient semitransparent and flexible devices was demonstrated by Han et al. reporting a white quantum dot (QD) LED with a maximum current efficiency of 18.2 cd A^{-1}, a maximum luminance value above 10 000 cd m^{-2} and an external quantum efficiency of 6.4%.[8]

Light-emitting electrochemical cells (LECs) currently represent a promising alternative to LED and OLED technologies as in their simplest form they consist only of a light-emitting active layer sandwiched between two electrodes.[14] The active layer is composed of a blend of an electroluminescent semiconductor,[15–17] a salt and an electrolyte.[18,19] Over the years, numerous efforts have already been made to improve the properties of the blend of conjugated polymers (CP) and small molecules,[15,20–22] and ligand design in ionic transition metal complexes (iTMCs),[23,24] in pursuit of long-lived, efficient, and bright devices. However, the literature is still relatively poor for semitransparent LECs with only a couple of examples reported, albeit using a top electrode that is either a conductive polymer or a nano array.[25,26]

In this work, we developed semitransparent iTMC-LECs using a TCO as both the top and the bottom electrodes. The top electrode was processed in a multilayer structure

L. Mardegan, A. Paliwal, K. P. S. Zanoni, D. Tordera, H. J. Bolink
Instituto de Ciencia Molecular (ICMol)
Universidad de Valencia
C/Catedrático J. Beltrán 2, Paterna (Valencia) 46980, Spain
E-mail: henk.bolink@uv.es

The ORCID identification number(s) for the author(s) of this article can be found under https://doi.org/10.1002/adom.202201953.

DOI: 10.1002/adom.202201953

composed of tin oxide (SnO_2) processed by atomic layer deposition (ALD) and ITO processed by pulsed laser deposition (PLD). The cathode was directly deposited on top of the organic active layer based on a yellow iridium(III) iTMC emitter, $[Ir(ppy)_2(dtb\text{-}bpy)][PF_6]$ (where ppy is 2-phenylpyridine and dtb-bpy is 4,4′-di-tert-butyl-2,2′-dipyridyl).[27] The energy levels of SnO_2 and the active material in the light-emitting layer are not aligned. Due to the operation mechanism of LECs involving ion migration to the electrode interface, this is not a problem. Furthermore, the combination of ALD and PLD offers the advantages of adjusting the deposition conditions, such as pressure and temperature, to provide a high-quality film, with precise control over thickness and composition. The possible harsh effects of the ALD and PLD during processing on the organic underlayers were examined. Transmittance, electroluminescence spectra (EL), and luminance output from both bottom and top side was measured. A very high transparency, above 75% over the visible spectra region (380 to 750 nm), was obtained in conjunction with a high electroluminescence above 200 cd m^{-2} which implies a very strong on/off contrast.

2. Results and Discussion

First, we developed the semitransparent top electrode for LEC devices. A fundamental condition for efficient light-emitting devices is to ensure the absence of shorts and leakage paths. TCOs represent the best choice in terms of transparency combined with a high conductivity, tunable electronic properties, and fabrication ease with several techniques. However, their deposition on organic thin films is not trivial as these materials are frequently deposited using harsh methods such as reactive ion sputtering or PLD. Even for ALD processes, the presence of reactive gasses and the needed temperatures can lead to undesired shorts. Additionally, it is important to have an energy matching interface between the light-emitting layer and the charge injection and electrode layers.[5,7] For PLD processes, the chamber pressure is a crucial factor because it determines the way the particles pack during the layer formation and, therefore, it affects its electrical properties. Generally, the lower the chamber pressure, the more conductive the TCO layer is, due to the enhanced bulk properties of the resultant film. However, it can also result in a higher number of shorts due to the higher kinetic energy of the TCO particles when impacting on the underlying layer. This effect has been recently demonstrated on perovskite solar cells where the ITO deposition pressure parameters were optimized.[28] Therefore, a higher chamber pressure needs to be used in the PLD process for the ITO deposition in order to minimize the damage to the samples. Based on this, we selected a chamber pressure of 0.042 mbar (with an O_2 partial pressure of 0.0076 mbar) for the deposition of the top ITO electrode via PLD. A 140 nm ITO layer deposited on glass under these conditions exhibited a sheet resistance of 140 Ω sq^{-1}. However, when deposited directly on the organic emitting layer in the LEC stack, it produced a considerable number of shorted devices.

To ensure there is no penetration of ITO in the thin film of the Ir(III) emitter, we employed an additional SnO_2 electron transport layer (ETL) via ALD. SnO_2 is gaining increased consideration for its use as a wide band gap semiconductor due to its high transmission and electrical properties combined with remarkable chemical stability and compatibility with several doping elements and fabrication techniques.[29] Recent works describe the use of SnO_2 as ETL in optoelectronic devices.[30–32] Regarding the ALD technique, the growth temperature and choice of the precursors are the key factors in order to achieve suitable film properties. However, for thermally sensitive materials, such as organics or organometallic semiconductors, it is imperative to reduce the growth temperature to a level at which this technique can be sustainably exploited. For our devices, we obtained SnO_2 films at a growth temperature of 90 °C without further annealing using tetrakis(diethylamino)tin (TDAT) and water as precursors.[33] The SnO_2 films were characterized by means of atomic force microscopy (AFM) and X-ray photoelectron spectroscopy (XPS). An AFM image of a thin SnO_2 film on a glass/ITO/PEDOT:PSS/Ir substrate (**Figure 1**a) reveals a very flat surface with an estimated mean roughness of 0.6 nm. Our results are in line with previous reports where SnO_2 was deposited at low temperature.[33–35] The XPS analysis (Figure 1b) reveals the formation of SnO_2,[33] with an element ratio close to

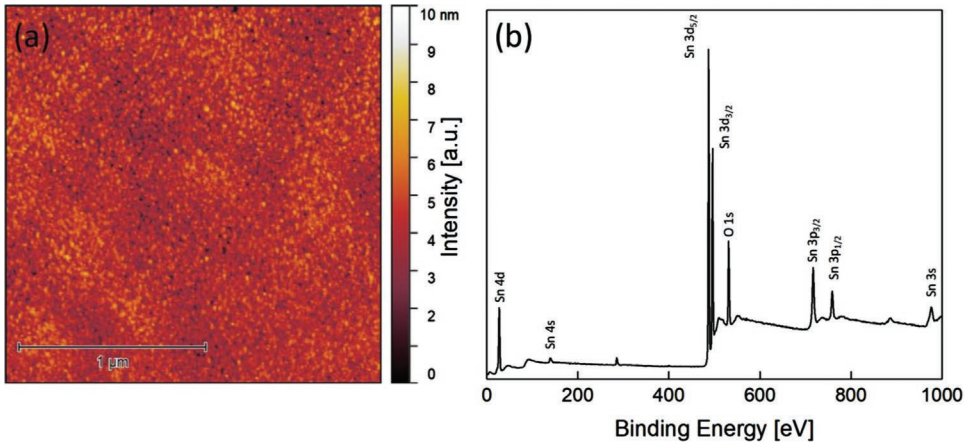

Figure 1. a) AFM topographic image of an ALD-deposited SnO_2 thin film on glass/PEDOT:PSS/Ir substrate. b) XPS survey of SnO_2 thin film on glass/ITO substrate.

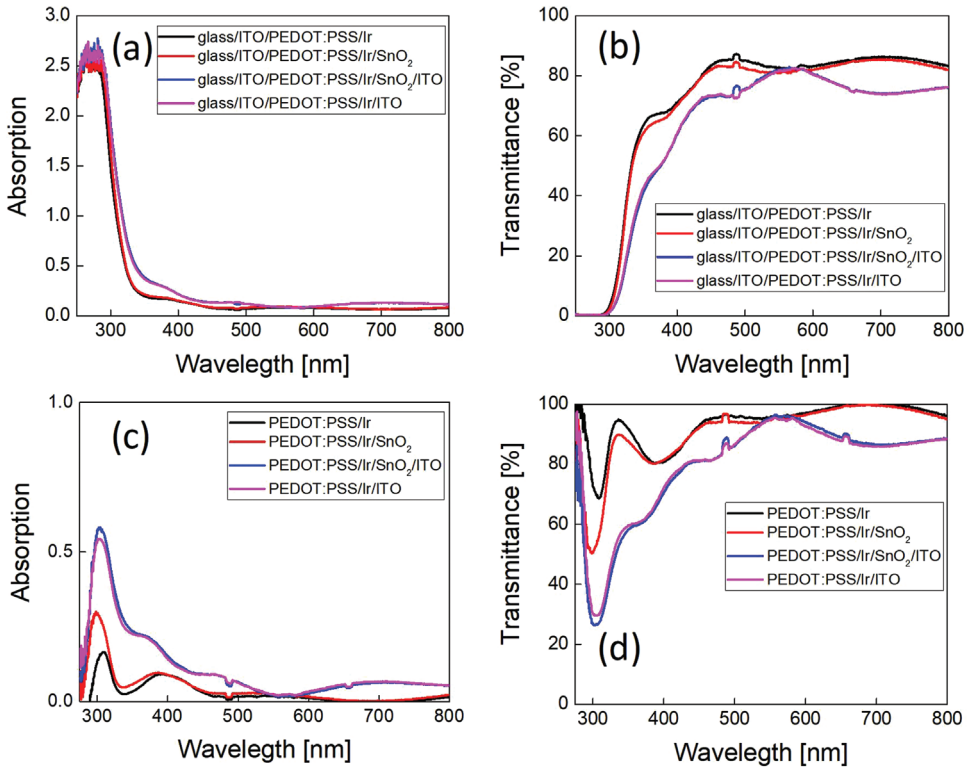

Figure 2. a) Absorbance and b) transmittance of the samples, before and after the SnO_2 and ITO layers deposition. c) Absorbance and d) transmittance of the same samples using a glass/ITO reference sample.

1:2 between Sn and O. Topographic AFM images were also collected for Ir deposited on glass/PEDOT:PSS and for ITO deposited on glass/PEDOT:PSS/Ir and glass/PEDOT:PSS/Ir/SnO_2 samples (Figure S1, Supporting Information) showing flat surfaces in all cases with mean roughness below 1.5 nm.

Thereafter, we proceeded to examine the effect of the deposited SnO_2 and ITO layers on the optical properties of the device stack. We prepared samples before and after the SnO_2 and ITO layers deposition, that is, glass/ITO/PEDOT:PSS/Ir, glass/ITO/PEDOT:PSS/Ir/SnO_2, glass/ITO/PEDOT:PSS/Ir/SnO_2/ITO, and glass/ITO/PEDOT:PSS/Ir/ITO, where Ir is the active layer composed of $[Ir(ppy)_2(dtb\text{-}bpy)][PF_6]$ and 1-butyl-3-methylimidazolium hexafluorophosphate $[BMIM][PF_6]$ in a molar ratio of 1:0.25. The thicknesses of SnO_2 and ITO were 20 and 140 nm, respectively. The absorbance and transmittance spectra of glass/ITO/PEDOT:PSS/Ir and glass/ITO/PEDOT:PSS/Ir/SnO_2 (**Figures 2**a,b, black and red curves, respectively) are superimposable and the addition of ITO slightly increases the absorption of light and consequently results in a decrease in transmission (Figures 2a,b, blue and pink curves, respectively). The full stack (blue curve) showed an average transmittance value of 75% within the visible spectrum range (380 to 750 nm) with a transmittance of 82% at the electroluminescence peak of 563 nm (discussed later and seen in Figure 4a). These measurements give important information about the features of the final device, however, they do not tell much about the intrinsic properties of the deposited layers because of the strong effect that the glass substrate has on the absorption. When glass and ITO from the substrate are not taken into consideration (Figure 2c,d), it is possible to observe that the SnO_2 and ITO deposition increases (decreases) the absorption (transmission), especially in the lower wavelength region between 300 and 400 nm of the spectra with respect to the Ir sample (black curve). This is in line with the absorption spectra measured for SnO_2 and ITO (Figure S2, Supporting Information).

Next, devices were fabricated in the following configuration: glass/ITO/PEDOT:PSS (80 nm)/$[Ir(ppy)_2(dtb\text{-}bpy)][PF_6]$:[BMIM][$PF_6$] (1:0.25) (80 nm)/$SnO_2$ (20 nm)/ITO (140 nm) (**Figure** 3a). After the cathode deposition, gold was thermally evaporated at the edges to supply an additional low resistance path to facilitate effective charge injection from the ITO cathode. As mentioned before, the direct deposition of ITO resulted in a large number of shorts while SnO_2 effectively acted as a buffer layer preventing these shorts. For this reason, we will focus our discussion only on the device configuration that includes the SnO_2 buffer layer. The semitransparent devices were also compared with standard fully reflective Al-cathode (100 nm) LECs. The iridium complex, $[Ir(ppy)_2(dtb\text{-}bpy)][PF_6]$, represented in Figure 3b, has been previously used as a yellow light-emitting material in iTMC-LECs and has displayed high stability and efficiency.[27,36] Images of the semitransparent device and the standard opaque device in their ON and OFF states are shown in Figure 3c–f showing the transparency of the transparent devices. To further highlight the transparency of these samples, pictures of transparent devices without the Au fingers were also taken and are shown in Figure S3, Supporting Information.

Both the transparent and opaque devices were characterized by applying a pulsed driving current of 100 A m^{-2}

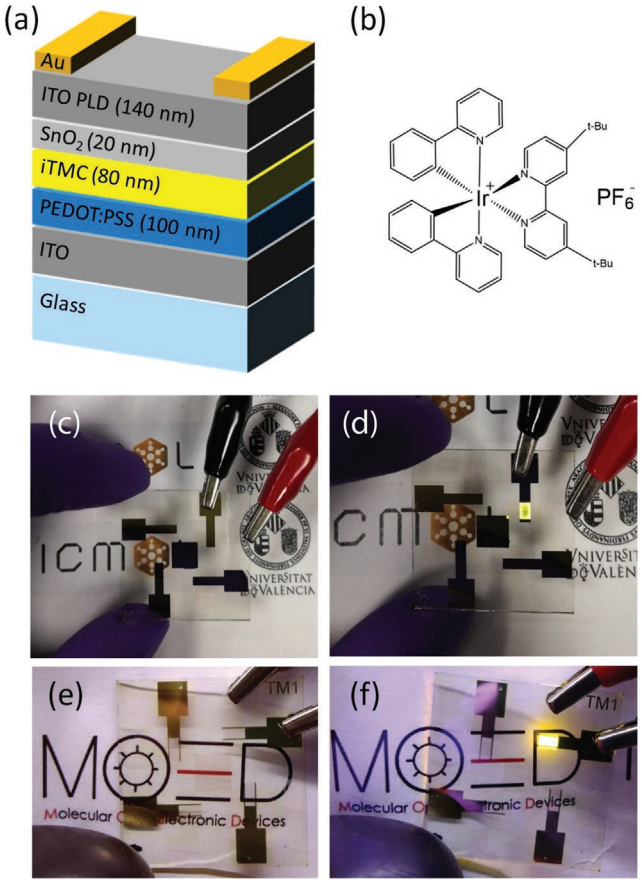

Figure 3. a) Architecture of the semitransparent devices. b) Chemical structure of the yellow Ir(III) emitter $[Ir(ppy)_2(dtb\text{-}bpy)][PF_6]$ used in this work. OFF states of the c) reference and e) semitransparent devices, and ON states of the d) reference and f) semitransparent devices.

(avg. 50 A m^{-2}) and monitoring their luminance and voltage evolution over time. The pulsed bias consisted of a block wave current at a frequency of 1000 Hz with a duty cycle of 50%. The luminance of the transparent devices was measured from top (SnO_2/ITO side) and bottom (glass/ITO side). The electroluminescence spectra of the standard and semitransparent devices through the bottom substrate were rather similar (**Figure 4**a). The EL peak from the semitransparent device is slightly blue-shifted when compared to the opaque reference device, with maxima of 563 and 571 nm, respectively. The observed blue-shift could be the result of a different light outcoupling for the opaque and transparent devices, where the light-emitting layer acts as a cavity in which the position of the emissive non-doped zone is governed by the choice of the cathode. The main figures of merit of both the opaque and transparent LEC are summarized in **Table 1**. The opaque device shows the evolution of luminance and voltage typical for LECs driven with a pulsed current (Figure 4b). In the first stages after applying the bias, the high resistance causes a high starting voltage. As the ionic species migrate within the thin film creating the electronic double layers (EDLs) the voltage quickly decreases while the luminance increases. The reference device reaches a maximum luminance value of 620 cd m^{-2} and a t_{50}, referred to as the time necessary to reach half of the maximum luminance, of 1120 h. The high luminance and the low pulsed driving current density make this device very efficient with a peak current efficiency (CE) value of 13.6 cd A^{-1} and a power efficiency (PE) of 8.9 lm W^{-1}. The semitransparent devices (Figure 4c,d), biased with the same average current density of 50 A m^{-2} and maintaining the same electrode polarity, show a similar performance. When measured from the bottom side, the luminance reached a value of 260 cd m^{-2} which is less than what is obtained for the opaque cells. This is primarily due to the loss of the reflecting electrode in the transparent devices. Indeed, when measured through the top ITO electrode, a luminance of 188 cd m^{-2} is obtained. Even though the sum of these two values is still below what is obtained for the opaque cell, the difference is not very large. We will comment on the possible origin of this difference in the next section. As a result of the lower luminance also the current efficacy and the power efficiency are lower in the transparent devices. The luminance values obtained from the bottom and top side are 260 and 188 cd m^{-2} which leads to CE and PE values of 5.2 and 4.0 cd A^{-1}, and 3.2 and 2.5 lm W^{-1}, for the bottom and top side, respectively. Finally, the t_{50} for the bottom side is 176 h while that for the top side is 118 h.

Several factors can contribute to the different luminance values observed for the bottom and top sides of the devices. The outcoupling of photons depends strongly on the refractive index of the layers the emitted light must pass through in order to escape from the device. With regard to SnO_2, several reports show that its electrical as well as optical properties depend on the deposition temperature and precursors used.[33,37] The refractive index is reported to be close to 1.9/2.0 when SnO_2 is deposited from TDAT and water at low temperatures (below 100 °C).[33] When driving the device and measuring from the bottom side (glass), the light is partially trapped because the glass substrate has a low refractive index of ≈1.5. For commercial ITO on glass substrates the reported refractive index is generally 1.8 but the ITO optical properties are strictly related to its crystallinity, resistivity, and surface morphology. For PLD deposition, these properties are controlled by changing chamber pressure and deposition temperature. It has been reported that room temperature depositions could lead to higher sheet resistance and refractive indices.[38,39] For our deposited ITO, due to the medium/high chamber pressure of 0.042 mbar (see Experimental Section) and room temperature, the final refractive index might be close to 2.0 or higher. The high refractive index of the top TCO electrode supports the outcoupling from the organic light-emitting material into the TCO layers, however because of the large contrast in indices between the TCOs and air (≈2 TCO:1 air) the light remains constrained within the outer TCOs layers. In order to exploit the advantage of using a high refractive index based outcoupling layer, nano arrays/lenses[40] would be required. In addition, internal reflections of the different layers of the stack and from the gold fingers evaporated around the device area could play an important role in determining the final light output from the top and bottom side. This difference in luminance measured from the bottom and top sides has also been confirmed by the simultaneous measurement with two equidistant photodiodes of the generated photocurrent by the two sides of the same pixel under a constant current bias of 50 A m^{-2} (Figure S4, Supporting Information). Although these results were obtained with a constant

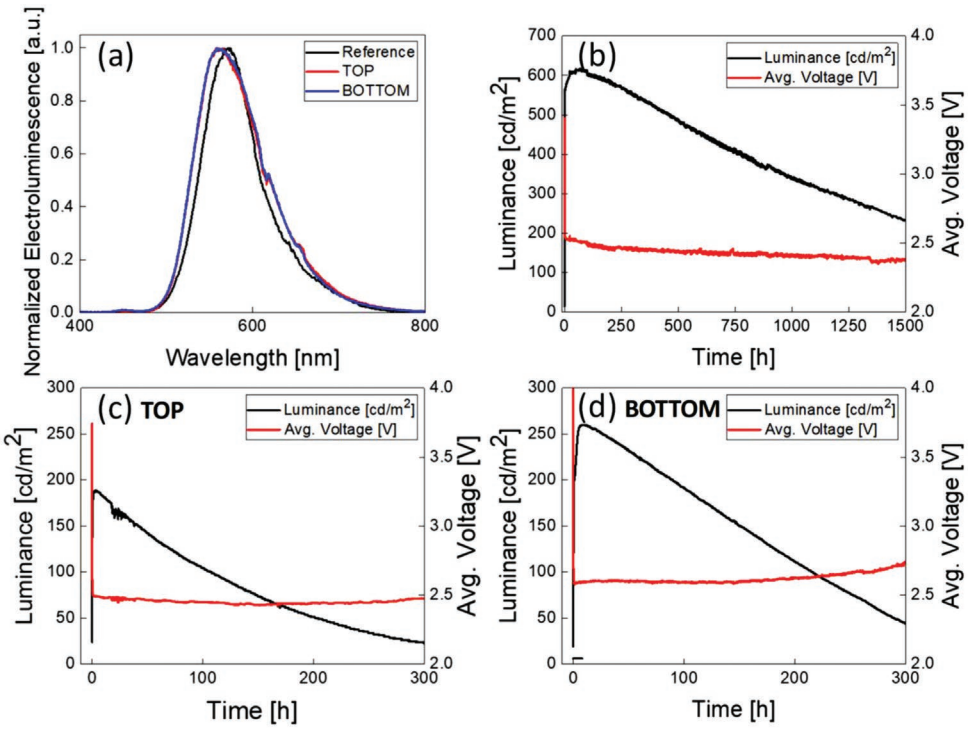

Figure 4. a) Electroluminescence of the standard Al-cathode and semitransparent devices, b) luminance and voltage over time of the standard Al-cathode device at an avg. current of 50 A m^{-2}. c,d) Luminance and voltage over time of the top and bottom sides of the transparent device driven at avg. current of 50 A m^{-2}.

bias, they are in agreement with the luminance versus time data showed in Figure 4. Differences between top and bottom emission were also previously reported in transparent OLED and QD-LED, and attributed to a difference in transparency between the top and bottom electrodes.[10,13]

Finally, a rough estimate of the overall performance of the semitransparent device (obtained as the sum of the top and bottom measurements) can be made. The overall luminance is 448 cd m^{-2} with a CE and PE of 9.2 cd A^{-1} and 5.7 lm W^{-1}. Another factor that could play a role in the performance of the semitransparent LEC device is the photoluminescence (PL) quenching as a consequence of the cathode deposition. To study this, the photoluminescence was measured to understand the interactions between the Ir thin film and the SnO_2 and ITO deposited layers. The PL was measured from both sides of the samples using an excitation wavelength of 340 nm in an integrating sphere, where bottom indicates that the sample was excited from the glass substrate side and top from the PLD-ITO cathode side (**Figure 5**a,b). Analyzing the bottom orientation (Figure 5a) we observe that the PL intensity suffers from both the ALD and PLD depositions. In the first case, a drop of the PL intensity of 19% is observed by the ALD-deposited SnO_2 thin layer (red curve). It is well known the ability of SnO_2[31,41–43] and other metal oxides based ETLs[44,45] to quench the PL at the semiconductor/TCO interface through exciton trapping and non-radiative energy transfer. Furthermore, a degradation of the Ir complex by the action of the nucleophilic water molecules and temperature during the ALD deposition could play a critical role.[23,24] The ITO deposition directly on the active Ir material dramatically increases the quenching to about 52% (pink curve). Here, the ITO deposition could be too harsh for the organic active layer, as seen on the number of resulting shorted devices. Surprisingly, we observe a remarkable decrease in the number of shorted cells upon SnO_2 insertion and, at the same time, the presence of an important interaction between the iTMC and the cathode as suggested by the intense PL quenching, around 48%, observed in the full-stack sample glass/ITO/PEDOT:PSS/Ir/SnO_2/ITO (blue curve). Second, we measured the samples from the top side (Figure 5b). The samples showed the same degree of quenching after the SnO_2 deposition (red curve), as expected. The addition of ITO in the Ir/ITO and Ir/SnO_2/ITO samples (pink and blue curves, respectively) follows the same trend as the bottom orientation, however with a higher degree of quenching of 74% and 65%, respectively.

Table 1. Figures of merit of the standard and transparent (T) cells driven at 50 A m^{-2} average bias current.

	Peak lum. [cd m^{-2}]	t_{50} [h]	CE [cd A^{-1}]	PE [lm W^{-1}]
Standard	620	1120	13.6	8.9
T-bottom side	260	176	5.2	3.2
T-top side	188	118	4.0	2.5
T-overall	448	—	9.2	5.7

3. Conclusion

In conclusion, in this work we have fabricated semitransparent iTMC-LECs by using a transparent top SnO_2/ITO contact processed by ALD and PLD, respectively. The devices had

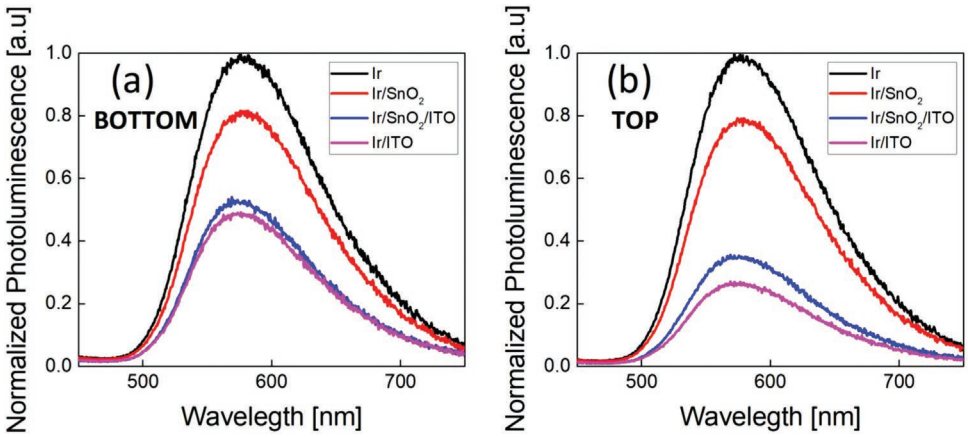

Figure 5. Photoluminescence from the a) BOTTOM side and b) TOP side obtained with an excitation wavelength of 340 nm of the iTMC film and with different metal oxide layers deposited on top of it.

a full-stack transparency of 75% over the visible spectrum (380 to 750 nm) with a transmittance of 82% at the electroluminescence peak of 563 nm. We were able to characterize the devices by measuring them from both sides. The devices showed excellent on/off ratio characterized by a high transmittance, and a luminance up to 260 cd m^{-2} coupled to lifetimes up to 176 h demonstrating the potential of these highly transparent light-emitting devices.

4. Experimental Section

Materials: Anhydrous acetonitrile (ACN) and 1-butyl-3-methylimidazolium hexafluorophosphate [BMIM][PF_6] were obtained from Sigma-Aldrich and stored under N_2 filled atmosphere. The Ir(III) complex, [Ir(ppy)$_2$(dtb-bpy)][PF_6], was synthesized following a previously reported procedure.[27]

Solution Preparation: [Ir(ppy)$_2$(dtb-bpy)][PF_6] solutions were made in ACN at a final concentration of 20 mg mL^{-1} and a molar ratio of 1:0.25 of [Ir(ppy)$_2$(dtb-bpy)][PF_6]:[BMIM][PF_6] was used. The ionic liquid (IL) solution was previously prepared in anhydrous ACN at a concentration of 10 mg mL^{-1} under inert atmosphere. The solvation of both the iTMC and IL in ACN as well as the final mixed solution were instantaneous and no further heating and stirring were needed.

Samples and Device Preparation: Pre-patterned indium tin oxide (ITO)-coated glass plates were used as transparent conductive substrates. They were subsequently cleaned ultrasonically in water-soap, water, and 2-propanol baths. After drying, the substrates were placed in a UV–ozone cleaner (Jelight 42–220) for 20 min. The ITO substrates were first coated with PEDOT:PSS and then with the iTMC-IL solution. Thicknesses of 100 and 80 nm were obtained, respectively. Before coating with the iridium complex, the PEDOT:PSS layers were annealed at 150 °C for 10 min. The iridium complex thin films were then annealed, instead, on a hotplate at 90 °C for 1 h under N_2 atmosphere. A 20 nm layer of SnO_2 was deposited by ALD using an Arradiance's GEMStar XT Thermal ALD system integrated into a nitrogen-filled glovebox. For that, the ALD chamber was heated to 90 °C, the bottle containing the Sn precursor (tetrakis(dimethylamino) tin, TDAT) was heated to 60 °C while the bottle of oxidizer (water) was not heated, and the precursor and oxidizer manifolds were heated to 115 and 140 °C, respectively. Prior to deposition, the tubes and valves in the manifolds were degassed three times by performing a series of 30 pulses with the bottles manually closed. The edges of the ITO contacts were protected with Dupont's polyimide Kapton tape and then the substrates were inserted in the ALD chamber, which was then evacuated. One ALD cycle consisted of consecutive purges of TDAT for 550 ms and water vapor for 200 ms, each followed by N2 purges of 30 and 105 s, respectively, to ensure the complete removal of the precursors from the ALD chamber (final growth per cycle: 1.5 Angs). Finally, 140 nm of ITO were deposited by Pulsed Laser Deposition technique (Solmates large area 200 mm PLD system) with a chamber pressure of 0.042 mbar and an O_2 partial pressure of 0.0076 mbar, controlled by a constant injection of an oxygen/argon gas mix, and at room temperature. This PLD tool is coupled to a N2 glovebox, to minimize any detrimental effects from O_2 and moisture on the performance of the finally produced devices. A Lightmachinery IPEX-700 KrF excimer laser (λ = 248 nm) was employed, setting the repetition rate at 25 Hz and a fluence of 1.5–1.7 J cm^{-2}. The source material for ITO deposition was a Sn:In_2O_3 ceramic target with 2:98 wt%. The substrates were taped to shadow masks to obtain the final deposition layouts. Shadow masks were used during the ITO deposition to obtain a final active area of 6 mm^2. To increase the conductivity of the ITO cathode, Au fingers of 50 nm were thermally evaporated at the side of the cathode without covering the active area of the cells. The final active area of the down side of the LEC is of 6 mm^2 while on the up side the active area measures 4.8 mm^2. For the reference devices, 100 nm Al cathode was deposited via thermal evaporation using a shadow mask. The final active area of the cells was of 6 mm^2. Samples on glass or glass/ITO substrates for photophysical and surface characterization followed exactly the same fabrication steps. The following samples were fabricated for the photophysical measures on glass/ITO substrates: PEDOT:PSS/Ir, PEDOT:PSS/Ir/SnO_2, PEDOT:PSS/Ir/SnO_2/ITO, and PEDOT:PSS/Ir/ITO.

Photophysical Measurements: The absorbance and transmittance were measured with an Avantes AvaLight-DS-S-BAL deuterium halogen light source and an Avantes AvaSpec-2048L spectrometer. While the photoluminescence was measured in an N-M01 integrated sphere and a FLS1000 Edinburg Spectrometer, the PL-lifetimes were measured with a Hamamatsu Quantaurus-Tau C11367 with an excitation LED light source of 365 nm and 1800 s measurement time in air.

Atomic Force Microscopy: AFM measurements were collected in a Multimode atomic force microscope (Veeco Instruments, Inc.). The images were obtained with a Si tip with frequency and K of ≈300 kHz and 40 $N{\cdot}m^{-1}$, respectively, using the tapping mode in air at room temperature. Images were recorded with a 0.5–1 Hz scan rate.

X-Ray Photoelectron Spectroscopy: The SnO_2 samples on glass substrates were analyzed with a Thermo Scientific K-alpha compact X-ray photoelectron spectrometer with a monochromatized Al K-alpha radiation of 1486.6 eV and a base pressure of 4×10^{-9} mbar.

Sheet Resistance Measurement: A manual four point resistivity probe equipment (Signatone S-301-4 PWK) and a Keithley were employed.

LECs Characterization: The devices were measured by applying a pulsed current density of 50 A m^{-2} while monitoring the voltage and luminance versus time by using a True Color Sensor MAZeT (MTCSiCT sensor) with a Botest OLT OLED Lifetime-Test system. The applied pulsed current consisted in block waves at a frequency of 1000 Hz with a duty cycle of 50%. As a result, the average current density and voltage were obtained by multiplying the values by the time-on (0.5 s) and dividing by the total cycle time (1 s). The sensor measured the average value of the luminance during the chosen duty cycle. The electroluminescence spectra were measured with an optical fiber connected to an Avantes AvaSpec-2048L spectrometer while driving the cell with a Botest OLT OLED Lifetime-Test system. The simultaneous photocurrent of the same pixel was recorded through two picoamperometers perpendicularly placed at the same distance from the pixel, while a constant current density of 50 A m^{-2} was applied with a Keithley. Thinner gold fingers were deposited on these devices to have the same active area from both dies. The LEC characterization was conducted under nitrogen atmosphere.

Supporting Information

Supporting Information is available from the Wiley Online Library or from the author.

Acknowledgements

The authors thank Jorge Ferrando for his technical support. The research leading to these results has received funding from the European Research Council (ERC) under the European Union's Horizon 2020 research and innovation programme (Grant agreement No. 834431), from Projects PCI2019-111829-2 and PID2021-126444OB-I00 funded by MCIN/AEI/10.13039/501100011033 and by the European Union, from Project CEX2019-000919-M funded by MCIN/AEI/10.13039/501100011033, and from Project PDC2021-121317-I00 funded by MCIN/AEI/10.13039/501100011033 and by the "European Union NextGenerationEU/PRTR". This work also received financial support from the Comunitat Valenciana (IDIFEDER/2018/061, CIGE/2021/027, and Prometeu/2020/077). K.P.S.Z. acknowledges funding from Comunitat Valenciana (APOSTD/2021/368). A.P. acknowledges his Grisolia grant from the Comunitat Valenciana (GRISOLIAP/2020/134).

Conflict of Interest

The authors declare no conflict of interest.

Data Availability Statement

The data that support the findings of this study are available from the corresponding author upon reasonable request.

Keywords

atomic layer deposition, high transmittance, light-emitting electrochemical cells, pulsed laser deposition, transparent devices

Received: August 22, 2022
Revised: September 8, 2022
Published online: October 6, 2022

[1] C. S. Buga, J. C. Viana, *Adv. Mater. Technol.* **2021**, *6*, 2001016.
[2] R. Pode, *Renewable Sustainable Energy Rev.* **2020**, *133*, 110043.
[3] M. G. Song, K. S. Kim, H. I. Yang, S. K. Kim, J. H. Kim, C. W. Han, H. C. Choi, R. Pode, J. H. Kwon, *Org. Electron.* **2020**, *76*, 105418.
[4] L. Liu, K. Cao, S. Chen, W. Huang, *Adv. Opt. Mater.* **2020**, *8*, 2001122.
[5] M. Morales-Masis, S. De Wolf, R. Woods-Robinson, J. W. Ager, C. Ballif, *Adv. Electron. Mater.* **2017**, *3*, 1600529.
[6] D. Li, W.-Y. Lai, Y.-Z. Zhang, W. Huang, *Adv. Mater.* **2018**, *30*, 1704738.
[7] E. Aydin, C. Altinkaya, Y. Smirnov, M. A. Yaqin, K. P. S. Zanoni, A. Paliwal, Y. Firdaus, T. G. Allen, T. D. Anthopoulos, H. J. Bolink, M. Morales-Masis, S. De Wolf, *Matter* **2021**, *4*, 3549.
[8] C. Y. Han, K. H. Lee, M. S. Kim, J. W. Shin, J. S. Kim, J. H. Hwang, T. Kim, M. S. Oh, J. Kim, Y. R. Do, H. Yang, *Org. Electron.* **2017**, *45*, 145.
[9] J. H. Oh, J. W. Park, *Phys. Status Solidi RRL* **2020**, *14*, 1900707.
[10] J. H. Oh, J. W. Park, *Org. Electron.* **2021**, *96*, 106252.
[11] Y. Yasuda, S. Kobayashi, T. Uchida, Y. Hoshi, *Thin Solid Films* **2020**, *698*, 137868.
[12] Y. J. Lee, J. H. Kim, J. N. Jang, I. H. Yang, S. N. Kwon, M. P. Hong, D. C. Kim, K. S. Oh, S. J. Yoo, B. J. Lee, W. G. Jang, *Thin Solid Films* **2009**, *517*, 4019.
[13] W. Wang, H. Peng, S. Chen, *J. Mater. Chem. C* **2016**, *4*, 1838.
[14] J. Xu, A. Sandström, E. M. Lindh, W. Yang, S. Tang, L. Edman, *ACS Appl. Mater. Interfaces* **2018**, *10*, 33380.
[15] S. Kanagaraj, A. Puthanveedu, Y. Choe, *Adv. Funct. Mater.* **2020**, *30*, 1907126.
[16] J. Gao, *ChemPlusChem* **2018**, *83*, 183.
[17] A. Mishra, M. Alahbakhshi, R. Haroldson, L. D. Bastatas, Q. Gu, A. A. Zakhidov, J. D. Slinker, *Adv. Opt. Mater.* **2020**, *8*, 2000226.
[18] J. Mindemark, L. Edman, *J. Mater. Chem. C* **2016**, *4*, 420.
[19] M. H. Bowler, A. Mishra, A. C. Adams, C. L. D. Blangy, J. D. Slinker, *Adv. Funct. Mater.* **2020**, *30*, 1906715.
[20] J. Mindemark, S. Tang, H. Li, L. Edman, *Adv. Funct. Mater.* **2018**, *28*, 1801295.
[21] J. Mindemark, S. Tang, J. Wang, N. Kaihovirta, D. Brandell, L. Edman, *Chem. Mater.* **2016**, *28*, 2618.
[22] L. Mardegan, C. Dreessen, M. Sessolo, D. Tordera, H. J. Bolink, *Adv. Funct. Mater.* **2021**, *31*, 2104249.
[23] C. E. Housecroft, E. C. Constable, *Coord. Chem. Rev.* **2017**, *350*, 155.
[24] C. Zhang, R. Liu, D. Zhang, L. Duan, *Adv. Funct. Mater.* **2020**, *30*, 1907156.
[25] E. Auroux, A. Sandström, C. Larsen, P. Lundberg, T. Wågberg, L. Edman, *Org. Electron.* **2020**, *84*, 105812.
[26] G. Qian, Y. Lin, G. Wantz, A. R. Davis, K. R. Carter, J. J. Watkins, *Adv. Funct. Mater.* **2014**, *24*, 4484.
[27] J. D. Slinker, A. A. Gorodetsky, M. S. Lowry, J. Wang, S. Parker, R. Rohl, S. Bernhard, G. G. Malliaras, *J. Am. Chem. Soc.* **2004**, *126*, 2763.
[28] K. P. S. Zanoni, A. Paliwal, M. A. Hernández-Fenollosa, P.-A. Repecaud, M. Morales-Masis, H. J. Bolink, *Adv. Mater. Technol.* **2022**, https://doi.org/10.1002/admt.202101747.
[29] G. K. Dalapati, H. Sharma, A. Guchhait, N. Chakrabarty, P. Bamola, Q. Liu, G. Saianand, A. M. Sai Krishna, S. Mukhopadhyay, A. Dey, T. K. S. Wong, S. Zhuk, S. Ghosh, S. Chakrabortty, C. Mahata, S. Biring, A. Kumar, C. S. Ribeiro, S. Ramakrishna, A. K. Chakraborty, S. Krishnamurthy, P. Sonar, M. Sharma, *J. Mater. Chem. A* **2021**, *9*, 16621.
[30] Q. Jiang, X. Zhang, J. You, *Small* **2018**, *14*, 1801154.
[31] H. Wang, H. Yu, W. Xu, Z. Yuan, Z. Yan, C. Wang, X. Liu, M. Fahlman, J. M. Liu, X. K. Liu, F. Gao, *J. Mater. Chem. C* **2018**, *6*, 6996.
[32] Y. Liu, S. Wei, G. Wang, J. Tong, J. Li, D. Pan, *Langmuir* **2020**, *36*, 6605.

[33] M. N. Mullings, C. Hägglund, S. F. Bent, *J. Vac. Sci. Technol., A* **2013**, *31*, 061503.
[34] J. Heo, A. S. Hock, R. G. Gordon, *Chem. Mater.* **2010**, *22*, 4964.
[35] D. Choi, J.-S. Park, *Surf. Coat. Technol.* **2014**, *259*, 238.
[36] E. Bandiello, M. Sessolo, H. J. Bolink, *J. Mater. Chem. C* **2016**, *4*, 10781.
[37] J.-H. Lee, M. Yoo, D. Kang, H.-M. Lee, W. Choi, J. W. Park, Y. Yi, H. Y. Kim, J.-S. Park, *ACS Appl. Mater. Interfaces* **2018**, *10*, 33335.
[38] H. Kim, J. S. Horwitz, A. Piqué, C. M. Gilmore, D. B. Chrisey, *Appl. Phys. A: Mater. Sci. Process.* **1999**, *69*, S447.
[39] A. Khodorov, M. Piechowiak, M. J. M. Gomes, *Thin Solid Films* **2007**, *515*, 7829.
[40] R. Liang, J. Dai, L. Xu, J. He, S. Wang, Y. Peng, H. Wang, L. Ye, C. Chen, *IEEE Trans. Electron Devices* **2018**, *65*, 2498.
[41] J. Mei, M. S. Bradley, V. Bulović, *Phys. Rev. B* **2009**, *79*, 235205.
[42] V.-H. Tran, H. Park, S. H. Eom, S. C. Yoon, S.-H. Lee, *ACS Omega* **2018**, *3*, 18398.
[43] L. Yan, Q. Xue, M. Liu, Z. Zhu, J. Tian, Z. Li, Z. Chen, Z. Chen, H. Yan, H.-L. Yip, Y. Cao, *Adv. Mater.* **2018**, *30*, 1802509.
[44] J. M. Caruge, J. E. Halpert, V. Wood, V. Bulović, M. G. Bawendi, *Nat. Photonics* **2008**, *2*, 247.
[45] V. Wood, M. J. Panzer, J. E. Halpert, J.-M. Caruge, M. G. Bawendi, V. Bulović, *ACS Nano* **2009**, *3*, 3581.